Origin of Dirac Cones in SiC Silagraphene: A Combined Density Functional and Tight-Binding Study

ARTICLE *in* JOURNAL OF PHYSICAL CHEMISTRY LETTERS · APRIL 2015

Impact Factor: 7.46 · DOI: 10.1021/acs.jpclett.5b00365

THE JOURNAL OF PHYSICAL CHEMISTRY Letters

Letter

pubs.acs.org/JPCL

Origin of Dirac Cones in SiC Silagraphene: A Combined Density Functional and Tight-Binding Study

Xuming Qin,[†,‡] Yi Liu,*[,†,§] Xiaowu Li,*[,‡] Jingcheng Xu,[§] Baoqian Chi,[‡] Dong Zhai,[†] and Xinluo Zhao[†]

[†]Department of Physics and Materials Genome Institute, Shanghai University, 99 Shangda Road, Shanghai 200444, P. R. China

[‡]Institute of Materials Physics and Chemistry, College of Sciences, Northeastern University, No. 3-11, Wenhua Road, Shenyang 110819, P. R. China

[§]School of Materials Science and Engineering, University of Shanghai for Science and Technology, 516 Jungong Road, Shanghai 200093, P. R. China

Supporting Information

ABSTRACT: The formation of Dirac cones in electronic band structures via isomorphous transformation is demonstrated in 2D planar SiC sheets. Our combined density functional and tight-binding calculations show that 2D SiC featuring C−C and Si−Si atom pairs possesses Dirac cones (DCs), whereas an alternative arrangement of C and Si leads to a finite band gap. The origin of Dirac points is attributed to bare interactions between Si−Si bonding states (valence bands, VBs) and C−C antibonding states (conduction bands, CBs), while the VB−CB coupling opens up band gaps elsewhere. A mechanism of atom pair coupling is proposed, and the conditions required for DC formation are discussed, enabling one to design a class of 2D binary Dirac fermion systems on the basis of DF calculations solely for pure and alternative binary structures.

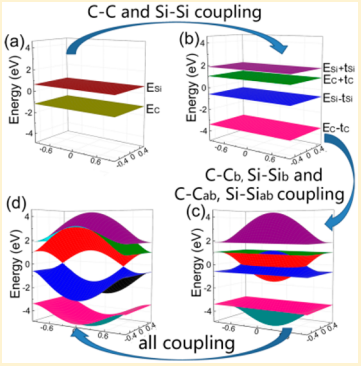

Two-dimensional (2D) monatomic carbon nanosheet—graphene[1] features Dirac cones (DCs) referring to the conical shapes whose points meet at Fermi energy levels in its electronic band structures. Electron or hole carriers around Dirac points are massless Fermions with k-independent Fermi velocity $v_F \approx 10^6$ ms^{-1} and obey linear energy dispersion relation $E = \hbar v_F k$ described by Dirac equations.[2,3] Dirac cones contribute to several intriguing properties of graphene including quantum electrodynamics-like behavior, anomalous integer quantum Hall effect,[4,5] as well as exceptional high carrier mobility up to 10^7 cm^2/(V s)[6] technologically critical for nanoelectronic applications. Silicene, a silicon analogy of graphene, also possesses electronic structures characterizing Dirac cones but slightly buckled atomic structures.[7−9] As an extension to 2D binary nanosheets, silicon carbides (SiC_x) dubbed silagraphenes exhibit a variety of metastable structures depending on both chemical compositions and arrangement patterns. One of the most studied 2D SiC_x, h-SiC (Si/C 1:1) with alternative Si and C arrangement,[10−19] is predicted to be a semiconductor. Silagraphenes with other stoichiometry have also been studied recently. SiC_2 featuring planar tetracoordinate Si units are metallic in both planar and tubular forms.[20] Three low-energy structures of SiC_3 were studied, among which one is metal and the other two are semimetals.[21,22] Other graphene-based derivatives, for example, chlorographene or janugraphene, are predicted to possess Dirac cones after chemical modification with Cl or H.[23]

The origin of the Dirac cone was initially attributed to graphene's honeycomb structure and hexagonal symmetry with equivalent sublattices. Nevertheless, it was recently claimed that these prerequisites were not necessary, as demonstrated in 6,6,12-graphyne,[24] chlorographene, or janugraphene.[23] Despite the increasing interest in Dirac fermion systems, the fundamental understanding of the origin of Dirac cone formation, especially for 2D binary system, is still far from completed. This work reports two new SiC (at 1:1 stoichiometry) silagraphene structures that possess Dirac cones. These Dirac fermion systems feature C−C and Si−Si atom pairs in contrast with the semiconducting SiC with alternative C and Si arrangements. Furthermore, we propose an atom pair coupling mechanism elucidating the formation of Dirac cones: The coupling between Si−Si π−π bonding states (valence band, VB) and C−C π−π antibonding states (conduction band, CB) opens up band gaps, whereas the VB and CB remain touched at the noncoupling Dirac points. Finally, we discuss the necessary conditions where the pair coupling mechanisms can be applied to search for other binary Dirac fermion systems.

In this work, density functional (DF) calculations were used to acquire optimized geometries and electronic structures, while analyses based on tight-binding (TB) approximations provided more physical insights. Most DF calculations were carried out at a GGA-PBE level using the plane-wave CASTEP program.[25]

Received: February 19, 2015
Accepted: March 25, 2015

DOI: 10.1021/acs.jpclett.5b00365
J. Phys. Chem. Lett. 2015, 6, 1333−1339

The ion−electron interaction is described using an ultrasoft pseudopotential with a cutoff energy 600 eV. k points sample the Brillouin zone in reciprocal space at a separation of 0.03 ($\times 2\pi$) Å^{-1} ($k = 2\pi/\lambda$ is adopted in this manuscript and the Supporting Information (SI).) More detailed computation parameters are described in Section S1 of the SI.

We studied all 10 possible types of SiC silagraphene structures with various Si/C arrangement patterns using an eight-atom rectangular unit cell, although some structures can be further reduced to smaller primitive cells according to symmetry. We started from various bulked structures and found two of the studied types have planar structures that are energetically most stable and possess Dirac cones. Both of these Dirac fermion systems contain C−C and Si−Si atom pairs connected by C−Si bonds dubbed t1 and t2-SiC (tetragonal primitive cell), respectively (Figure 1b,c). Both structures have

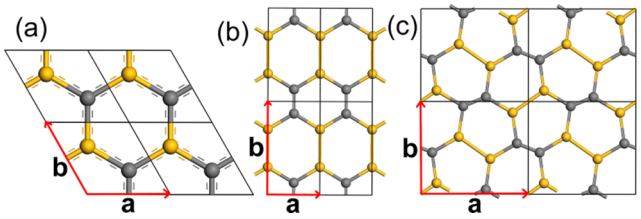

Figure 1. Atomic structures for (a) h-SiC, (b) t1-SiC, and (c) t2-SiC. The yellow balls represent Si and the gray balls represent C.

C−C and Si−Si atom pairs as building units but differ in their relative arrangements: all C−C and Si−Si pairs align parallel to each other in t1-SiC[26] with *Pmmm* symmetry but distribute more isotropically in t2-SiC with *Pba*2 symmetry. For the sake of comparison, the silagraphene with alternative arrangement of C and Si atoms dubbed h-SiC[27] is shown in Figure 1a. The other seven types of SiC structures are either semiconducting or metallic, whose most stable structures are all bulked, as discussed in Section S2 of the SI.

To evaluate stabilities of the studied silagraphene structures, we calculated the formation energy per atom as $E_f = (\Sigma_i E_i - E_f)/n$, where E_f is the total energy per cell, E_i is the energy of the ith isolated atom, and n is the total number of atoms per cell. E_f of h-SiC is 7.076 eV, close to the average value 7.021 eV between graphene (9.259 eV) and silicene (4.784 eV). E_f of t1-SiC and t2-SiC is 6.745 and 6.763 eV, respectively, ∼0.3 eV lower than that of h-SiC. The t1-SiC and t2-SiC are less stable than h-SiC probably due to the mismatch between optimal bond lengths of C−C (1.42 Å in graphene) and Si−Si (2.28 Å in silicene). The C−C bonds in t1-SiC and t2-SiC are stretched, but Si−Si bonds are compressed by ∼0.02 to 0.03 Å relative to those in graphene and silicene, and the C−Si bonds are elongated by 0.03 Å compared with that of h-SiC. The stabilities of t1-SiC and t2-SiC are further confirmed by our phonon calculations, where negligible (<10 cm^{-1}) imaginary frequency was found. Moreover, the ab initio molecular dynamics at the NPT ensemble show that both t1-SiC and t2-SiC structures remain intact without collapse up to 1000 K and 1 atm pressure for 5 ps. More detailed results of structure, energy, phonon, and MD can be found in Table S1 and Figures S4−S7 of the SI.

Next, we investigate the electronic properties of h, t1, and t2-SiC silagraphene. The h-SiC is predicted to be a semiconductor with a band gap of 2.584 eV at a GGA-PBE level and 3.761 eV using more accurate hybrid functional B3LYP (Section S1 in the SI). For AB binary systems with alternative A and B arrangements, there exist only two sublattices; the band gap is related directly to the different onsite energies between C and Si in the TB picture, referred to as a "point coupling" mechanism hereafter. (See more detailed DFT and TB results of h-SiC in Section S3 and Figure S8 in the SI.) Apparently, the band gap disappears when the onsite energy difference becomes zero in 2D unitary systems such as graphene, silicene, and germanene[8] and even in binary SiGe.[28] Indeed, the DOS and orbital calculated by DFT show that the VB mainly consists of C-2p orbital, while the CB mainly consists of Si-3p orbital. These results are also consistent with previous literature reports.[11,12,14,29]

Although h-SiC exhibits semiconducting characters, t1 and t2-SiC are found to possess Dirac cones evidenced by Figure 2a,f and Sections S4−S7 of the SI. It is intriguing that Dirac

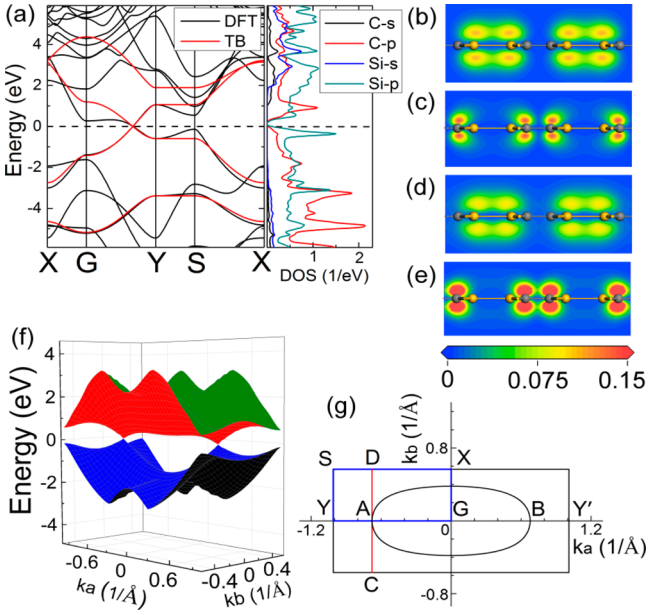

Figure 2. (a) Band structures and density of states of t1-SiC calculated by DFT (black) and TB (red). VB orbital cross-section through (b) Si−Si pairs and (c) C−C pairs perpendicular to the plane of t1-SiC. CB orbital cross-section through (d) Si−Si pairs and (e) C−C pairs perpendicular to the plane of t1-SiC. (f) VB and CB in total Brillouin zone of t1-SiC calculated by DFT. (g) Brillouin zone of t1-SiC in reciprocal space. The ellipse-like closed ring is the intersection of the VB and CB from TB when neglecting the coupling between Si−Si$_b$ and C−C$_{ab}$ as well as that between Si−Si$_{ab}$ and C−C$_b$. Fermi energies are shifted to zero in all above cases.

cones can be obtained solely by rearranging Si and C atoms without changing stoichiometry and 2D honeycomb structures.

To clarify the origin of Dirac cones of t1-SiC, we performed TB analyses by considering only p_z orbital interactions between the nearest-neighbor atoms because they have major contributions to the VB and CB, as indicated by DFT-DOS (Figure 2a). The Hamiltonian can be written as

$$H = \begin{pmatrix} E_C & -t_C & 0 & -t[e^{-ik\cdot(a+b)} + e^{-ik\cdot b}] \\ -t_C & E_C & -t(1+e^{-ik\cdot a}) & 0 \\ 0 & -t(1+e^{ik\cdot a}) & E_{Si} & -t_{Si} \\ -t[e^{ik\cdot(a+b)} + e^{ik\cdot b}] & 0 & -t_{Si} & E_{Si} \end{pmatrix} \quad (1)$$

where E_C and E_{Si} are the onsite energies of C and Si and t_C, t_{Si}, and t are the hopping energies of C−C, Si−Si, and C−Si,

DOI: 10.1021/acs.jpclett.5b00365
J. Phys. Chem. Lett. 2015, 6, 1333−1339

respectively. We obtained the TB parameters by fitting to reproduce the DFT band structures: $E_C = -1.164$ eV, $E_{Si} = 0.649$ eV, $t_C = 2.225$ eV, $t_{Si} = 1.241$ eV, and $t = 1.433$ eV. Then, we solved the secular equation to acquire the TB band structures, consistent with the DFT results (Figures 2 and 3 and more details in Section S4 in the SI).

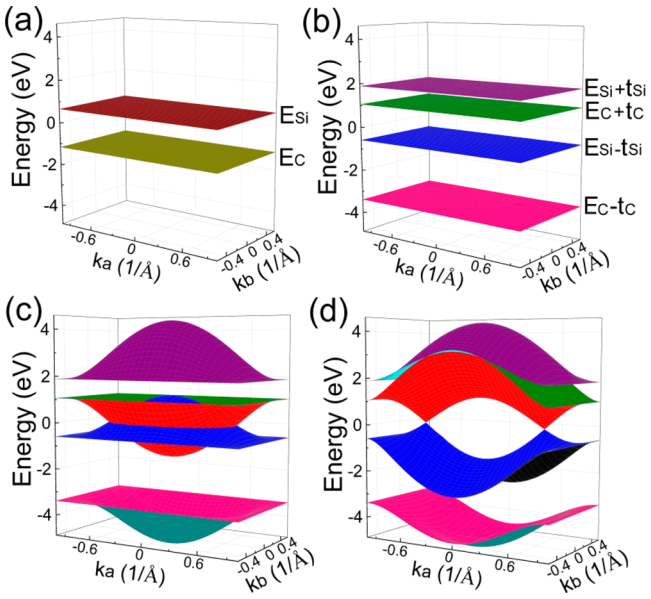

Figure 3. Formation of Dirac cones illustrated stepwise in the 3D band structures of t1-SiC calculated by TB. (a) Ignoring all of the couplings leads to only the C and Si onsite energies. (b) Considering only the coupling of C−C and that of Si−Si leads to four flat energy levels. (c) Considering only the coupling between C−C_b and Si−Si_b as well as that between C−C_{ab} and Si−Si_{ab} leads to the intersection of VB and CB. (d) Considering all couplings leads to the formation of Dirac cones.

To understand the formation of Dirac cones, we analyzed the TB Hamiltonian matrix. Because the two pairing C or Si atoms have the same onsite energies, the coupling of C−C or Si−Si is strong and thus considered first. We applied a unitary transformation S to H as follows

$$H' = S^{+}HS = \begin{pmatrix} E_C - t_C & 0 & -t(1+e^{-ik\cdot a})(1+e^{-ik\cdot b})/2 & -t(1+e^{-ik\cdot a})(-1+e^{-ik\cdot b})/2 \\ 0 & E_C + t_C & -t(1+e^{-ik\cdot a})(1-e^{-ik\cdot b})/2 & t(1+e^{-ik\cdot a})(1+e^{-ik\cdot b})/2 \\ -t(1+e^{ik\cdot a})(1+e^{ik\cdot b})/2 & -t(1+e^{ik\cdot a})(1-e^{ik\cdot b})/2 & E_{Si} - t_{Si} & 0 \\ -t(1+e^{ik\cdot a})(-1+e^{ik\cdot b})/2 & t(1+e^{ik\cdot a})(1+e^{ik\cdot b})/2 & 0 & E_{Si} + t_{Si} \end{pmatrix} \quad (2)$$

where

$$S = \frac{1}{\sqrt{2}} \begin{pmatrix} 1 & -1 & 0 & 0 \\ 1 & 1 & 0 & 0 \\ 0 & 0 & 1 & -1 \\ 0 & 0 & 1 & 1 \end{pmatrix}$$

If the C−Si couplings are neglected, the diagonal elements of H' lead to four flat energy levels (Figure 3b), among which $E_C - t_C$ is the energy of C−C bonding states (C−C_b), $E_C + t_C$ the C−C antibonding states (C−C_{ab}), $E_{Si} - t_{Si}$ the Si−Si bonding states (Si−Si_b), and $E_{Si} + t_{Si}$ the Si−Si antibonding states (Si−Si_{ab}). According to the DFT-derived TB parameters, $E_C + t_C$ is higher than $E_{Si} - t_{Si}$. The real band structures would be acquired by including the further couplings between the four energy levels. Now we consider the couplings along various high-symmetry paths:

(a) When $\boldsymbol{k}\cdot\boldsymbol{a} = \pm\pi$, only the diagonal elements are nonzero. So the four energy levels do not couple to each other and remain unchanged along the corresponding path YS in Figure 2a,g.

(b) When $\boldsymbol{k}\cdot\boldsymbol{b} = \pm\pi$, only couplings between C−C_{ab} and Si−Si_b exist, together with those between C−C_b and Si−Si_{ab}. So the gaps between VB and CB increase along the corresponding path SX in Figure 2a,g.

(c) When $\boldsymbol{k}\cdot\boldsymbol{b} = 0$, couplings exist between C−C_b and Si−Si_b as well as between C−C_{ab} and Si−Si_{ab}. Consequently, the VB moves up and the CB shifts down along the corresponding path GY in Figure 2a,g, leading to the VB and CB intersecting each other.

(d) When $\boldsymbol{k}\cdot\boldsymbol{a} = 0$, the couplings in (b) and (c) both exist, leading to the nonzero band gap along the path XG in Figure 2a,g.

Then, we extend the TB analyses to the whole Brillouin zone in the reciprocal space:

First, we only consider the coupling between C−C_b and Si−Si_b as well as that between C−C_{ab} and Si−Si_{ab} that make the VB bend upward and the CB bend downward, respectively. So VB and CB intersect at the Fermi surface (Figure 3b,c). The intersection curve crosses the path GY (GY′) at A (B) point in Figure 2g.

Next, we include the coupling between C−C_{ab} and Si−Si_b as well as that between C−C_b and Si−Si_{ab}, leading to the separation between VB and CB along the intersection curve; however, the VB and CB barely couple along the path GY (GY′), including the A (B) point. Consequently, the VB and CB meet only at the A and B points and open up gaps elsewhere. Therefore, the two Dirac cones form, as seen in Figures 2f and 3d.

In the previously described TB analyses, CB and VB are mainly constructed by C−C_{ab} and Si−Si_b, respectively. These TB pictures are supported by our DFT calculations. The electron orbital results (Figure 2b−e) indicate that VB and CB mainly consist of Si−Si bonding states and C−C antibonding states.

The electron/hole velocities of t1-SiC were calculated on the basis of the band structures, compared with those of graphene and silicene (Table 1). The electron velocities of silagraphene lie roughly between graphene and silicene and exhibit anisotropic features. As shown in Figure 3c, both v_v(GA) and v_c(AY) are the slope of the CB at the A point, originated from the coupling between C−C_{ab} and Si−Si_{ab} states. Similarly, both v_c(AG) and v_v(YA) are the slopes of the VB at A point, caused by the coupling between C−C_b and Si−Si_b states. $v_{v,c}$(CA) and

Table 1. Electron Velocity, v_c, and Hole Velocity, v_v, of t1-SiC, t2-SiC, Graphene, and Silicene Predicted by DFT at a GGA-PBE level

	v_v (10^6 m/s)				v_c (10^6 m/s)			
	GA	YA	CA	DA	AG	AY	AC	AD
t1-SiC	0.58	0.34	0.60	0.60	0.32	0.59	0.60	0.60
t2-SiC	0.50	0.65	0.56	0.56	0.65	0.52	0.55	0.55
	v_v (10^6 m/s)		v_c (10^6 m/s)	
	GK		MK		KG		KM	
graphene	0.84		0.82		0.84		0.82	
silicene	0.54		0.52		0.54		0.52	

DOI: 10.1021/acs.jpclett.5b00365
J. Phys. Chem. Lett. 2015, 6, 1333−1339

$v_{v,c}$(AD) are associated with the strength of coupling between the VB and CB. Therefore, the anisotropic features of these electron velocities are attributed to their different origins revealed by the TB analyses. The Fermi velocities that should have been equal occasionally appear slightly different due to numerical uncertainty in linear fitting. For example, v_c(AG) and v_v(YA) of t1-SiC that are 0.32 and 0.34 ($\times 10^6$ m/s), respectively, should be regarded as equal.

On the basis of the mechanistic understanding previously described, we can further discuss the conditions required for the formation of Dirac cones in other AB binary systems. Given that $E_A > E_B$, where E_A and E_B are the onsite energy of A and B, respectively, the band energy levels should follow the following inequality

$$E_A - t_A < E_B + t_B \text{ or } E_A - E_B < t_A + t_B \tag{3}$$

Moreover, the strong coupling between VB and CB is necessary, leading to

$$\sqrt{\frac{1}{4}(E_A + t_A - E_B - t_B)^2 + 4t^2} + \sqrt{\frac{1}{4}(E_A - t_A - E_B + t_B)^2 + 4t^2} > t_A + t_B \tag{4}$$

Now we discuss how inequality 4 can be obtained. First, the CB and VB must cross to form Dirac cones. On the basis of eq 2, we know that the strongest couplings occur at the G point between B−B and A−A antibonding states as well as between B−B and A−A bonding states. At the G point, the energy band generated from the coupling between B−B and A−A antibonding states is

$$E_1 = \frac{1}{2}(E_A + t_A + E_B + t_B) - \sqrt{\frac{1}{4}(E_A + t_A - E_B - t_B)^2 + 4t^2} \tag{5}$$

The energy band generated from the coupling between B−B and A−A bonding states is

$$E_2 = \frac{1}{2}(E_A - t_A + E_B - t_B) + \sqrt{\frac{1}{4}(E_A - t_A - E_B + t_B)^2 + 4t^2} \tag{6}$$

The CB and VB crossover requires $E_1 < E_2$, and thus inequality 4 can be obtained. Let

$$T = \sqrt{\frac{1}{4}(E_A + t_A - E_B - t_B)^2 + 4t^2} + \sqrt{\frac{1}{4}(E_A - t_A - E_B + t_B)^2 + 4t^2} \tag{7}$$

Then, inequality 4 can be rewritten as

$$T > t_A + t_B \tag{8}$$

For inequality 8, we can do further analysis as follows. According to the definition of T in inequality 7

$$T > \sqrt{4t^2} + \sqrt{4t^2} = 4t \tag{9}$$

Therefore, inequality 8 must be satisfied if

$$2t > \frac{t_A + t_B}{2} \tag{10}$$

Inequality 10 normally can be satisfied, and thus inequality 4 or 8 can be readily satisfied as well. Consequently, inequality 3 becomes the most critical condition for DC formation.

Next, we show how to use inequalities 3 and 4 to search for other AB binary systems with Dirac cones. As examples, we examine whether t1-BN, t2-BN, t1-GeC, t2-GeC, t1-GeSi, and t2-GeSi (see Figure 4) possess Dirac cones using the procedures described later.

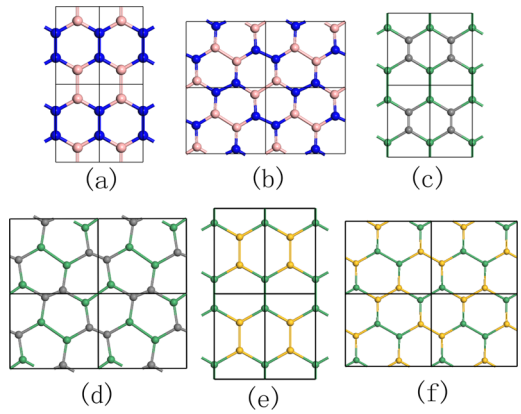

Figure 4. Atom structures of (a) t1-BN, (b) t2-BN, (c) t1-GeC, (d) t2-GeC, (e) t1-GeSi, and (f) t2-GeSi.

To examine the conditions of inequality 3 and 4 or 8, we need to evaluate the TB parameters $E_A - E_B$, $t_A + t_B$, and T. To this end, we calculated the band structures of AB systems with alternating A and B, pure A, and pure B to acquire these TB parameters by fitting against DFT band structures. The atom structures of these elementary systems are shown in Figure 5, and the corresponding band structures are shown in Figure 6.

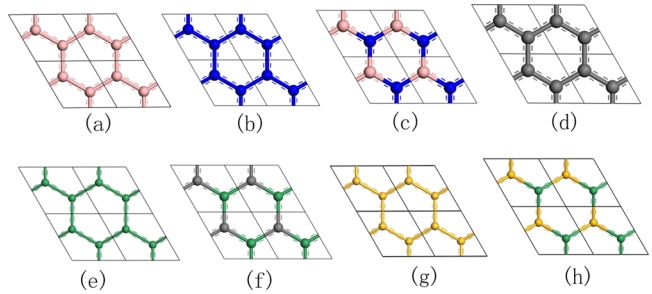

Figure 5. Atom structures of (a) h-BB, (b) h-NN, (c) h-BN, (d) graphene, (e) h-GeGe, (f) h-GeC, (g) silicene, and (h) h-GeSi.

On the basis of eqs 3 and 4 in the SI, we can write the formula of band structure derived from the coupling between p_z orbitals by TB for h-AB (or h-AA or h-BB) structures

$$E = \frac{1}{2}(E_A + E_B) \pm \sqrt{\frac{1}{4}(E_A - E_B)^2 + |H_{12}|^2} \tag{11}$$

where

$$|H_{12}|^2 = t^2\{3 + 2\cos(\boldsymbol{k}\cdot\boldsymbol{a}) + 2\cos(\boldsymbol{k}\cdot\boldsymbol{b}) + 2\cos[\boldsymbol{k}\cdot(\boldsymbol{a} + \boldsymbol{b})]\} \tag{12}$$

$|H_{12}|^2 = 0$ at K point, and the absolute value of energy difference between the two bands derived from the coupling between p_z

DOI: 10.1021/acs.jpclett.5b00365
J. Phys. Chem. Lett. 2015, 6, 1333−1339

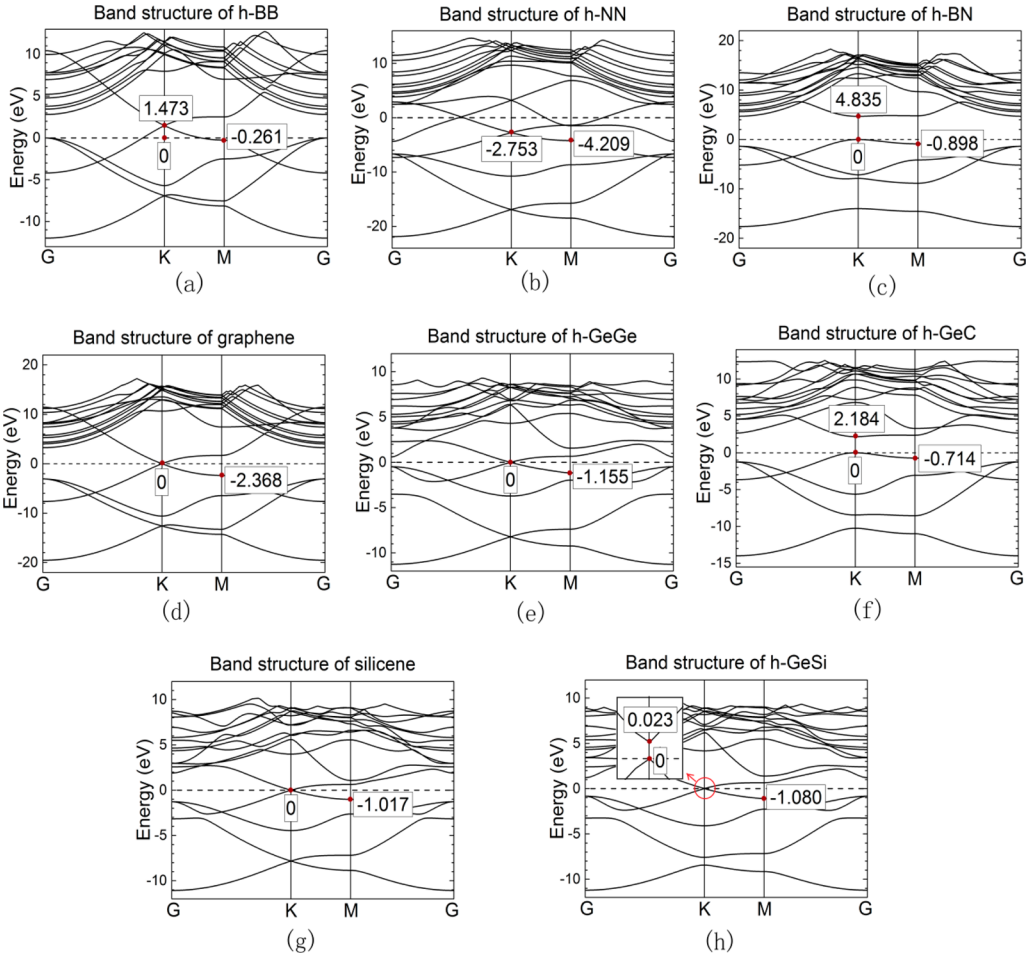

Figure 6. Band structures of AB, A, and B systems calculated by DFT where A or B are B, N, C, Si, and Ge elements.

orbitals is $E_A - E_B$. At M point, $|H_{12}|^2 = t^2$, and the lower energy band is

$$E_M = \frac{1}{2}(E_A + E_B) - \sqrt{\frac{1}{4}(E_A - E_B)^2 + t^2} \quad (13)$$

Therefore, using the energy values at K and M in the DFT band structures (see Figure 6), we can obtain the TB parameters $E_A - E_B$, t_A, t_B, t_{AB}, and T as listed in Table 2.

Table 2. Hopping Energy, Onsite Energy Differences, and the Parameter T of SiC, BN, GeC, and GeSi Systems

AB	$E_A - E_B$ (eV)	t_A (eV)	t_B (eV)	t_{AB} (eV)	$t_A + t_B$ (eV)	T (eV)
SiC[a]	2.63	1.02	2.37	1.64	3.39	7.17
BN	4.84	1.73	1.46	2.27	3.19	10.29
GeC	2.18	1.16	2.37	1.44	3.53	6.26
GeSi	0.02	1.16	1.02	1.09	2.18	4.37

[a]Parameters of SiC are from the band structures of graphene, silicene, and h-SiC calculated by DFT.

On the basis of the calculated parameters in Table 2, we can obtain the following inequalities:

(a) $E_{Si} - E_C < t_{Si} + t_C < T$ for the SiC systems
(b) $E_B - E_N > t_N + t_B < T$ for the BN systems
(c) $E_{Ge} - E_C < t_{Ge} + t_C < T$ for the GeC systems
(d) $E_{Ge} - E_{Si} < t_{Ge} + t_{Si} < T$ for the GeSi systems

According to the conditions of inequality 3 and 4 or 8, we make predictions that t1-SiC, t2-SiC, t1-GeC, t2-GeC, t1-GeSi, and t2-GeSi possess Dirac cones but t1-BN and t2-BN do not.

The TB model parameters that were acquired by the DF calculations of A, B, and alternative AB systems may be different from those acquired by the DF calculation of t1-BN, t2-BN, t1-GeC, t2-GeC, t1-GeSi, and t2-GeSi; however, all of these systems are honeycomb monolayer structures with the same stoichiometry, so the parameters obtained from the model systems can be reasonably used in predictions. Indeed, the band structures of t1-BN, t2-BN, t1-GeC, t2-GeC, t1-GeSi, and t2-GeSi calculated by DFT confirm our predictions, as shown in Figure 7, validating the prediction procedures of Dirac cone formation.

The case studies previously discussed demonstrate that the formation of Dirac cone in AB binary systems should satisfy the inequality conditions 3 and 4. Next, we discuss the possible range of hopping energies t_C and t_{Si} that lead to the DC formation as follows.

Inserting the TB parameters into inequality 3 and 4, we obtain scaling factors of 0.523 and 1.802 as the lower and upper limits, respectively, for both t_C and t_{Si}, when t_C/t_{Si} ratio and the other parameters are fixed. Moreover, the C−Si hopping energy $t > 0.708$ eV is necessary to make the VB and CB intersect or to satisfy inequality 4 when the other parameters are fixed. These inequality conditions were further verified via TB calculations by varying hopping energy parameters as well as DF calculations by changing C−Si, C−C, and Si−Si bond lengths

DOI: 10.1021/acs.jpclett.5b00365
J. Phys. Chem. Lett. 2015, 6, 1333−1339

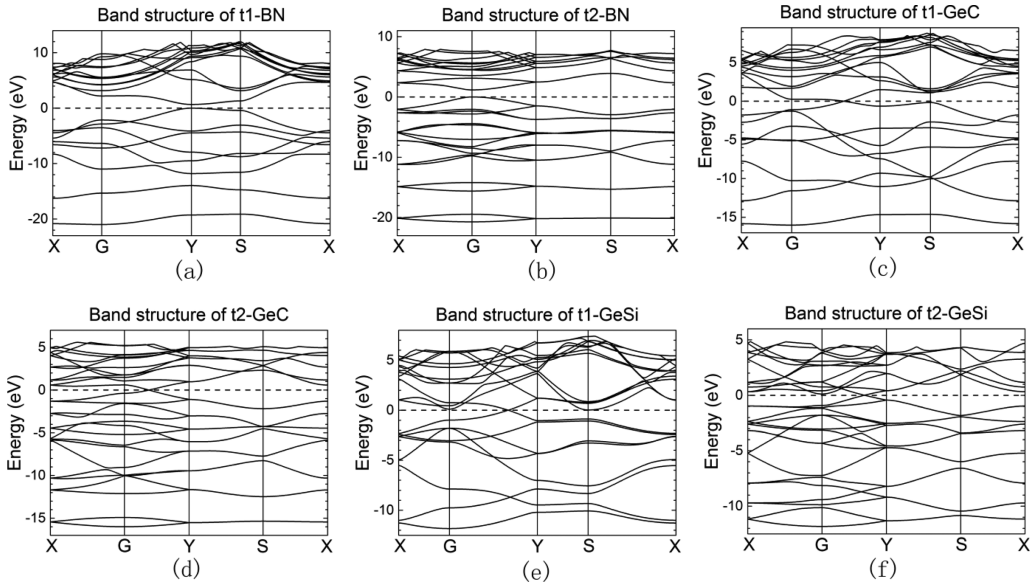

Figure 7. Band structures of t1-BN, t2-BN, t1-GeC, t2-GeC, t1-GeSi, and t2-GeSi calculated by DFT.

(Figure S9 in Section S5 in the SI). These results also indicate that Dirac cones cannot be easily destroyed when C−Si, C−C, and Si−Si bond lengths vary, implying that DC formation is robust to deformation subject to strain possibly induced by the misfit with substrate or external tension/compression load or pressure (Figure S10 in the SI).

t2-SiC also consists of C−C and Si−Si pairs but arranges more isotropically than t1-SiC. t2-SiC also possesses Dirac cone due to possibly the same origin as t1-SiC. (Detailed DFT results and TB analyses can be found in Sections S7 and S8 in the SI.) The electron/hole velocities of t2-SiC are close to those of t1-SiC but more isotropic (Table 1).

In summary, the formation of Dirac cones via atom pairing can be conceptually divided into three steps: (1) The nearest C−C or Si−Si interactions plus their onsite energies lead to four flat energy bands: C−C_b, Si−Si_b, C−C_{ab}, and Si−Si_{ab}. (2) Including the pair−pair interactions between Si−Si_b and C−C_b bands enlarges the energy separation between them. Similarly, the couplings between C−C_{ab} and Si−Si_{ab} pairs increase the energy differences between the two bands. Consequently, the Si−Si_b band moves up while the C−C_{ab} band shifts down, leading to intersection of the two bands along an ellipse-like closed ring in the reciprocal space. (3) Introducing the interactions between Si−Si_b and C−C_{ab} separates the intersected valence bands and conduction bands, except for one or more *k* points where coupling barely exists. These noncoupling k points still connect VB and CB, forming the so-called Dirac cones. In short, the selective coupling between VB and CB leads to the formation of Dirac cones in siligraphenes. Here the formation of C−C and Si−Si atom pairs is critical to the origin of Dirac cones. The Dirac point shifts along the GY direction in the Brillouin zone depending on the strength of C−Si or C−C and Si−Si bonds, revealing strain effects on the electronic structures.

Finally, we propose the point coupling and pair coupling mechanisms of Dirac cone formation. The point coupling mechanism features atom−atom couplings, elucidating why graphene, silicene, and germanene have Dirac cones but SiC[14] and BN[30] with alternative element arrangement do not. The pair coupling mechanism states that AA and BB atom pair formation leads to Dirac cones in a binary AB system if (1) A has a higher onsite energy than B, (2) AA bonding state is lower than BB antibonding state, and (3) AB coupling is strong enough. Introducing the inhomogeneous atom redistribution, the atom pair coupling mechanism opens up a new avenue to design heterogeneous binary Dirac fermion systems.

■ ASSOCIATED CONTENT

Supporting Information

More detailed computation parameters; the atom structures and band structures of the other seven SiC structures studied in this work; more detailed results of structure, energy, phonon, and MD; TB analyses; DFT band structures of h- and t2-SiC; orbitals of h, t1, and t2-SiC; TB calculations with various hopping energy parameters and DF calculations with various bond lengths of t1-SiC; influence of uniaxial tension on the band structure of t1-SiC. This material is available free of charge via the Internet at http://pubs.acs.org.

■ AUTHOR INFORMATION

Corresponding Authors

*E-mail: yiliu@shu.edu.cn (Y.L.)
*E-mail: xwli@mail.neu.edu.cn (X.L.).

Notes

The authors declare no competing financial interest.

■ ACKNOWLEDGMENTS

We acknowledge financial support from "Shanghai Pujiang Talent" program (12PJ1406500), "Shanghai High-tech Area of Innovative Science and Technology (14521100602)", STCSM; "Key Program of Innovative Scientific Research" (14ZZ130) and "Key Laboratory of Advanced Metal-based Electrical Power Materials", the Education Commission of Shanghai Municipality; and State Key Laboratory of Heavy Oil Processing, China University of Petroleum (SKLOP201402001). X.L. acknowledges the Fundamental Research Funds for the Central University of China (grant nos. N110105001 and N120505001). X.Z. acknowledges the National Natural Science Foundation of China (grant nos. 51202137, 61240054, and 11274222). Computations were carried out using Hujiang HPC

DOI: 10.1021/acs.jpclett.5b00365
J. Phys. Chem. Lett. 2015, 6, 1333−1339

facilities at USST, Shanghai Supercomputer Center and National Supercomputing Center in Shenzhen, P.R. China.

REFERENCES

(1) Novoselov, K. S.; Geim, A. K.; Morozov, S. V.; Jiang, D.; Zhang, Y.; Dubonos, S. V.; Grigorieva, I. V.; Firsov, A. A. Electric Field Effect in Atomically Thin Carbon Films. *Science* **2004**, *306*, 666−669.
(2) Semenoff, G. W. Condensed-Matter Simulation of a Three-Dimensional Anomaly. *Phys. Rev. Lett.* **1984**, *53*, 2449−2452.
(3) Castro Neto, A. H.; Guinea, F.; Peres, N. M. R.; Novoselov, K. S.; Geim, A. K. The Electronic Properties of Graphene. *Rev. Mod. Phys.* **2009**, *81*, 109−162.
(4) Geim, A. K.; Novoselov, K. S. The Rise of Graphene. *Nat. Mater.* **2007**, *6*, 183−191.
(5) Novoselov, K. S.; Geim, A. K.; Morozov, S. V.; Jiang, D.; Katsnelson, M. I.; Grigorieva, I. V.; Dubonos, S. V.; Firsov, A. A. Two-Dimensional Gas of Massless Dirac Fermions in Graphene. *Nature* **2005**, *438*, 197−200.
(6) Neugebauer, P.; Orlita, M.; Faugeras, C.; Barra, A.-L.; Potemski, M. How Perfect Can Graphene Be? *Phys. Rev. Lett.* **2009**, *103*, 136403.
(7) Aufray, B.; Kara, A.; Vizzini, S.; Oughaddou, H.; Léandri, C.; Ealet, B.; Le Lay, G. Graphene-Like Silicon Nanoribbons on Ag(110): A Possible Formation of Silicene. *Appl. Phys. Lett.* **2010**, *96*, 183102.
(8) Cahangirov, S.; Topsakal, M.; Aktürk, E.; Sahin, H.; Ciraci, S. Two- and One-Dimensional Honeycomb Structures of Silicon and Germanium. *Phys. Rev. Lett.* **2009**, *102*, 236804.
(9) Guzmán-Verri, G. G.; Lew Yan Voon, L. C. Electronic Structure of Silicon-Based Nanostructures. *Phys. Rev. B* **2007**, *76*, 075131.
(10) Sun, X. H.; Li, C. P.; Wong, W. K.; Wong, N. B.; Lee, C. S.; Lee, S. T.; Teo, B. K. Formation of Silicon Carbide Nanotubes and Nanowires via Reaction of Silicon (from Disproportionation of Silicon Monoxide) with Carbon Nanotubes. *J. Am. Chem. Soc.* **2002**, *124*, 14464−14471.
(11) Bekaroglu, E.; Topsakal, M.; Cahangirov, S.; Ciraci, S. First-Principles Study of Defects and Adatoms in Silicon Carbide Honeycomb Structures. *Phys. Rev. B* **2010**, *81*, 075433.
(12) Garcia, J. C.; de Lima, D. B.; Assali, L. V. C.; Justo, J. F. Group IV Graphene- and Graphane-Like Nanosheets. *J. Phys. Chem. C* **2011**, *115*, 13242−13246.
(13) He, X. J.; He, T.; Wang, Z. H.; Zhao, M. W. Neutral Vacancy-Defect-Induced Magnetism in SiC Monolayer. *Physica E* **2010**, *42*, 2451−2454.
(14) Zhao, K.; Zhao, M. W.; Wang, Z. H.; Fan, Y. C. Tight-binding Model for the Electronic Structures of SiC and BN Nanoribbons. *Physica E* **2010**, *43*, 440−445.
(15) Kuzubov, A. A.; Eliseeva, N. S.; Krasnov, P. O.; Tomilin, F. N.; Fedorov, A. S.; Tolstaya, A. V. Calculating the Energy of Vacancies and Adatoms in a Hexagonal SiC Monolayer. *Russ. J. Phys. Chem. A* **2012**, *86*, 1091−1095.
(16) Gori, P.; Pulci, O.; Marsili, M.; Bechstedt, F. Side-dependent Electron Escape from Graphene- and Graphane-Like SiC Layers. *Appl. Phys. Lett.* **2012**, *100*, 043110.
(17) Morbec, J. M.; Rahman, G. Role of Vacancies in the Magnetic and Electronic Properties of SiC Nanoribbons: An ab initio Study. *Phys. Rev. B* **2013**, *87*, 115428.
(18) Lin, X.; Lin, S. S.; Xu, Y.; Hakro, A. A.; Hasan, T.; Zhang, B. L.; Yu, B.; Luo, J. K.; Li, E.; Chen, H. S. Ab initio Study of Electronic and Optical Behavior of Two-Dimensional Silicon Carbide. *J. Mater. Chem. C* **2013**, *1*, 2131−2135.
(19) Kuzubov, A. A.; Eliseeva, N. S.; Krasnov, P. O.; Tomilin, F. N.; Fedorov, A. S.; Tolstaya, A. V. Possibility of a 2D SiC Monolayer Formation on Mg(0001) and MgO(111) Substrates. *Russ. J. Phys. Chem. A* **2013**, *87*, 1332−1335.
(20) Li, Y. F.; Li, F. Y.; Zhou, Z.; Chen, Z. F. SiC_2 Silagraphene and Its One-Dimensional Derivatives: Where Planar Tetracoordinate Silicon Happens. *J. Am. Chem. Soc.* **2011**, *133*, 900−908.
(21) Ding, Y.; Wang, Y. L. Geometric and Electronic Structures of Two-Dimensional SiC_3 Compound. *J. Phys. Chem. C* **2014**, *118*, 4509−4515.
(22) Zhao, M. W.; Zhang, R. Q. Two-Dimensional Topological Insulators with Binary Honeycomb Lattices: SiC_3 Siligraphene and Its Analogs. *Phys. Rev. B* **2014**, *89*, 195427.
(23) Ma, Y. D.; Dai, Y.; Huang, B. B. Dirac Cones in Two-Dimensional Lattices: Janugraphene and Chlorographene. *J. Phys. Chem. Lett.* **2013**, *4*, 2471−2476.
(24) Malko, D.; Neiss, C.; Viñes, F.; Görling, A. Competition for Graphene: Graphynes with Direction-Dependent Dirac Cones. *Phys. Rev. Lett.* **2012**, *108*, 086804.
(25) Clark, S. J.; Segall, M. D.; Pickard, C. J.; Hasnip, P. J.; Probert, M. J.; Refson, K.; Payne, M. C. First Principles Methods Using CASTEP. *Z. Kristallogr.* **2005**, *220*, 567−570.
(26) Wang, L.; Sun, H. Thermal Conductivity of Silicon and Carbon Hybrid Monolayers: a Molecular Dynamics Study. *J. Mol. Model.* **2012**, *18*, 4811−4818.
(27) Avramov, P. V.; Fedorov, D. G.; Sorokin, P. B.; Sakai, S.; Entani, S.; Ohtomo, M.; Matsumoto, Y.; Naramoto, H. Intrinsic Edge Asymmetry in Narrow Zigzag Hexagonal Heteroatomic Nanoribbons Causes their Subtle Uniform Curvature. *J. Phys. Chem. Lett.* **2012**, *3*, 2003−2008.
(28) Zhou, H. C.; Zhao, M. W.; Zhang, X. M.; Dong, W. Z.; Wang, X. P.; Bu, H. X.; Wang, A. Z. First-Principles Prediction of a New Dirac-Fermion Material: Silicon Germanide Monolayer. *J. Phys.: Condens. Matter* **2013**, *25*, 395501.
(29) Banerjee, S.; Majumder, C. Conformers of Hydrogenated SiC Honeycomb Structure: A First Principles Study. *AIP Adv.* **2013**, *3*, 082136.
(30) Topsakal, M.; Aktürk, E.; Ciraci, S. First-Principles Study of Two- and One-Dimensional Honeycomb Structures of Boron Nitride. *Phys. Rev. B* **2009**, *79*, 115442.

DOI: 10.1021/acs.jpclett.5b00365
J. Phys. Chem. Lett. 2015, 6, 1333−1339